Applied Thermal Engineering 258 (2025) 124684



Contents lists available at ScienceDirect

Applied Thermal Engineering

journal homepage: www.elsevier.com/locate/apthermeng



Research Paper

Negative Joule heat effect on supercapacitor module

Zhongze Li [a], Chaojie Cui [a,*], Zhenzhen Ye [a], Guangpei Wang [b], Tong Wang [b,*], Weizhong Qian [a,*]

[a] Department of Chemical Engineering, Tsinghua University, 100084 Beijing, China
[b] Science and Technology Strategy Research Center, Huadian Electric Power Research Institute Co., Ltd., Beijing 100039, China

ARTICLE INFO

Keywords:
Joule Heat
Infrared thermography
Thermal behavior
Supercapacitor modules

ABSTRACT

Joule heat as the main heat source in high-power operation of supercapacitor modules, needs to be carefully considered in thermal management. The sufficient discussion on the temperature characteristics of supercapacitor modules, especially those containing auxiliary electronic components during operation is of importance. Here we reported the Joule heat effect on a supercapacitor module integrated on a circuit board in the charge and discharge cycles by an *in situ* Infrared imaging method. Temperature rise of total components including wires, circuit board, welding pint, resistor and capacitor cell could be simultaneously imaged with a sensitivity of 0.2–0.3 °C. Upon charge–discharge cycles from 5C-60C, Joule heat on these electronic components was discovered. The thermal transfered from the connected wires to the circuit board and finally to the cell, which significantly increased the temperature rise (from 9.3 °C to 19.6 °C at 60C) and temperature difference (9.6 °C at 60C) of different capacitors in modules. Further simulation results indicated that Joule heat on the circuit board was 2–3 times that of the capacitors in the module. Such additional heat flow without suitable cooling system would result an accelerated capacitance decay of the module. Therefore, a suitable module structure and thermal management strategy needed to be designed to minimize the Joule heat generation of such electronic components.

1. Introduction

With the rapid development of renewable electricity grid from the solar or wind energy, the frequency modulation system is highly desirable for the stable operation, as overcoming the drawbacks from the time and local region limitation of solar and wind energy. Lithium ion batteries (LIBs) have been widely used in recent years, and there have been continuous studies to further improve their theoretical capacity and cycle life through material system optimization [1]. Meanwhile, supercapacitors (SCs), one of the most powerful devices with high power density and superlong life time, owing to the double layer capacitance driven by the adsorption effect of porous materials for storing energy physically without releasing the obvious reaction heat [2–8], are also applied for frequency modulations not only in the portable electronics (in the electric vehicles or in the wind mill [4,5]) where only single SCs cells or very small SCs modules with absolute low power and energy capacitance needed, but also in the frequency modulation system for renewable electricity grid calls for the power up to 1 MW to 10 MW even more (For example, "5MW SC + 15 MW LIB hybrid energy storage and frequency regulation system " and "500 MW/1000MWh independent energy storage project" was developed in 2023, detailed introduction refer to SI-1). The thermal management (or heat accumulation) based on the SCs modules for such large systems is rarely reported to this date, which maybe become a crucial issue, considering SCs modules works at a far larger current condition with unexpected high frequency.

The emerging smart battery or SC is based on the signal system of various SCs or various batteries by physical connections like a complicated module or network [9], which can achieve a sensitive detection of the conditions of SCs or batteries. Apparent, rapid feedback of smart battery or SC system depends on the highly frequent charging mode, which is similar to that of a SC module and may have the similar thermal management problem. In addition, one SC module is consisted of various single cells connected with wires, or integrated on a circuit board via the tandem or parallel connection manner. SCs system up to MW scale is built with the various SC modules following the similar connection system. However, for SCs, existing research mostly focused on the energy storage principle of materials with less research on its heating characteristics and thermal management systems [10] and most of them

* Corresponding authors.
E-mail addresses: cuicj06@tsinghua.edu.cn (C. Cui), tong-wang@chder.com (T. Wang), qianwz@mail.tsinghua.edu.cn (W. Qian).

https://doi.org/10.1016/j.applthermaleng.2024.124684
Received 1 July 2024; Received in revised form 15 October 2024; Accepted 18 October 2024
Available online 19 October 2024
1359-4311/© 2024 Elsevier Ltd. All rights are reserved, including those for text and data mining, AI training, and similar technologies.

mainly focus on the measurement of individual heat generation and the heating principle at the material scale [11–16]. For SC module, although there was study on its cooling strategy and structure design [17–21], the research on systems containing circuit board and auxiliary electronic components, which were essential during actual system operation were still lack. In recent years, the working conditions of SC systems have become more and more stringent, mainly manifested in the expansion of system scale and the increase of high-power working time. Heating characteristics at the system scale need to be considered. In addition, accurate and rapid measurement methods should also be adopted to strengthen management and fully monitor possible fault points.

In the present work, we reported the negative Joule heat effect owing to the wire connection on the SCs modules. By using an *in situ* Infrared temperature imaging method with 0.2 °C accuracy, it was able to record the joule heat via the wire connection on a circuit board. Such heat was so high to exert a direct heat transport from the wires to each cell, arising the rapid thermal elevation of the cell, far exceeding the heat by the adsorption–desorption charge. As a result, a fast capacitance decay was observed for module charged at 60-100C. And slow temperature recovery inside the cell after 40–60C charge was found. The far high accuracy, as compared to thermal couple, ensured the finding of any risks in time. In addition, these findings suggested high priority on the management of joule heat so as to cool the circuit board instantly and reduce the use of connecting wires as low as possible. The phenomena revealed by *in situ* imaging method provided new insight on the thermal management of the module, as well as providing the suggestions for Battery Management System (BMS) strategy.

2. Experimental

2.1. Instrument

Cells used are commercial cylinder-type Electric Double Layer Capacitor (EDLC) with the diameter of 35.5 mm and height of 60 mm (produced by Jiangsu Zhongtian Technology Co., Ltd., ZTT). The electrode material was activated carbon (YP-50) and the organic electrolyte was ACN-TEABF$_4$. The SCs can operated at 2.7–2.85 V, inner resistance < 3 mΩ. The cell passed the high temperature aging test (continuous test at 65 °C for 1500 h). The test module (ZSS 54 V 36F) included 40 cells with an operating voltage of 54 V and total capacitance of 36F. Its mass was 4.8 kg, energy density was around 2.6 Wh/kg and power density was 0.5 kW/kg. The front side and back side of module were shown in Fig. 1a and 1b.

The module had an integrated positive pole and negative pole (Fig. 1b). As shown in Fig. 1c, B point was labeled as the core position of the circuit board. Other 1,2,3,4 points were labeled as C1, C2, C3 and C4 with different positions, respectively. Set (x, y) represents the position of the cell in module in Fig. 1c, then C1 at (5,1), C2 at (4,2), C3 at (3,3), C4 at (3,4) and B between (2,4), (2,5), (3,4) and (3,5). Meanwhile, environmental temperature was recorded. The environmental temperature and the temperature profiles of the whole circuit board could be obtained with different C-rates.

Infrared camera was produced by Hikmicro (HM-TD2067T-6/X). It had a resolution of 640*512, working at 50 Hz. Temperature could be imaged in the range of −20–150 °C and in the distance from 0.6 m to 5 m. Images could be directly produced by the camera and treated by the software.

Electrochemical test was performed with CE-6001n Battery Test System (NEWARE, Shenzhen China). The voltage range was 0–200 V for charge and 5–200 V for discharge with the accuracy of 0.02 % Full Scale (FS). The current range was 1–200 A with the accuracy of 0.05 % FS. The overall power of the instrument was 40 kW.

2.2. Calculation and simulation

Quantitatively, gross thermal energy of Joule heat could be described by Eq. (1) and thermal energy for accumulation can be described by Eq. (2):

$$Q = I^2Rt \tag{1}$$

$$Q = mCp\Delta T \tag{2}$$

where R represents the equivalent series resistance (ESR) [10], Cp was the specific heat capacitance and ΔT was the temperature increase. Heat balance of Joule heating was shown in Eq. (3)

$$I^2Rt = Q_{cooling} + mCp\Delta T \tag{3}$$

According to Eq. (3), joule heat could be transferred to the environment ($Q_{cooling}$) and accumulated by wires and cells ($mCp\Delta T$). In the temperature range of 10–100 °C without blowing, heat transfer via the convection and irradiation were both insignificant. If further consider that at the beginning of charge, the ΔT was quite small, the Eq. (3) could be simplified and $Q_{cooling}$ could be eliminated and $I^2Rt = mCp\Delta T$ could be

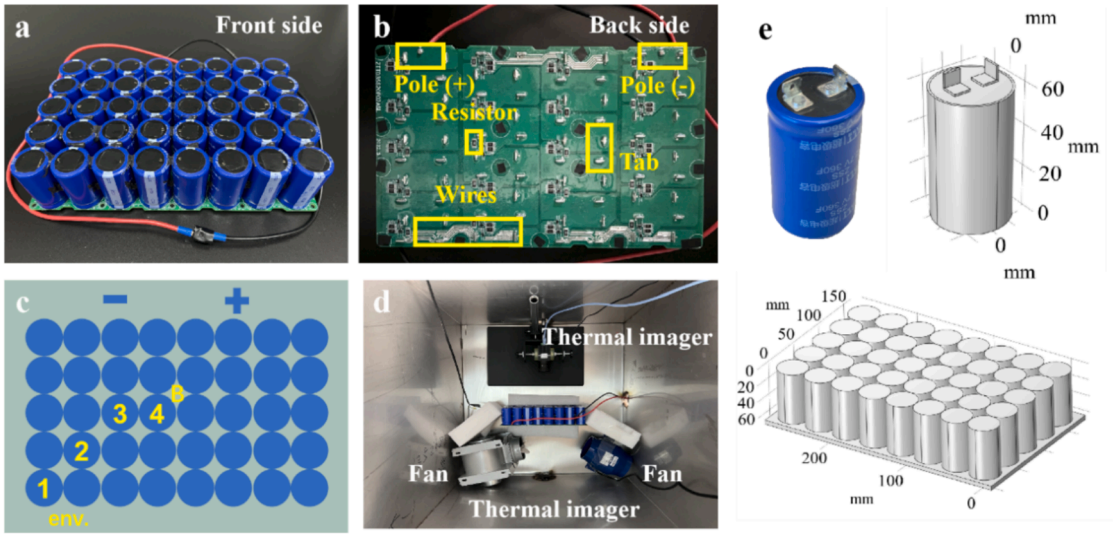


Fig. 1. The tested SCs modules via the Infrared image system and simulation model. (a) Photo of SCs modules; (b) photo of the circuit board where SCs were fixed on it; (c) illustration of eight point for temperature imaging(negative tab, positive tab, B: central point; C1-C4: SCs, E: environmental condition;); (d) photo of infrared thermal imager, SCs modules and two fans; (e) photo of single SC and simulation model of single SC and module.

established.

To quantitatively compare the heat generation of circuit boards and cells, a module heat generation model was established. Models were created for individual cell and module based on their actual dimensions. Including electrode materials, aluminum casing, circuit board, etc., the model was shown in Fig. 1e and corresponding material properties were shown in Table SI-3. The model only considered irreversible heat and temperature rise. For individual cell, current was applied at the tab and heat generation was described by Eq. (1).

For module, on the basis of individual cell modeling, the circuit

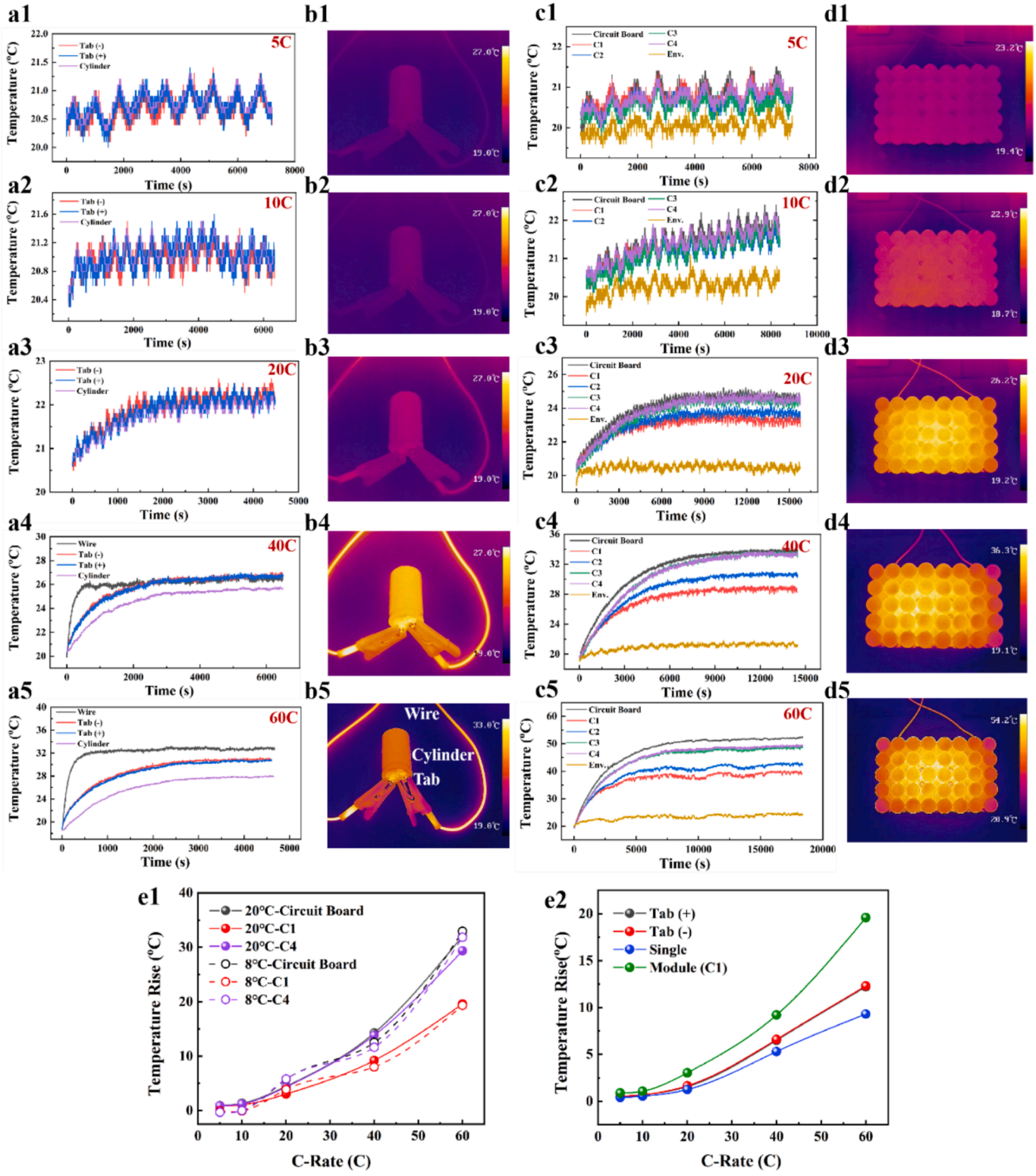


Fig. 2. Thermal behaviors of single cell and module at the environmental temperature of 20 °C. (a) temperature curve of single cell (wire upon joule heat at 40C and 60C, tabs and cylinder at 5–60C); (b) infrared image of single cell at 5–60C; (c) temperature curve of module (circuit board, C1-C4 and environment at 5–60C). (d) infrared image of module at 5–60C; (e1) Comparison of the temperature elevation of SCs under different environmental temperatures; (e2) Comparison of the temperature elevation of single cell and cell in SCs module (edge position, C1) under environmental temperature of 20 °C.

board was considered as an additional body heat source and the heat generation follows Eq. (1). Assuming that a portion of the heat came from the circuit board was used for overall heating, and another portion was used for causing temperature differences between each cells. Considering a appropriate boundary heat dissipation conditions to make the simulation results close to the experimental at 60C. Appling different proportions (depending on the contact area between the cell and environment) of heat dissipation boundary conditions to cells in the module according to their different locations to simulate their different natural cooling situations. The ambient temperature was 20 °C. All heat dissipation boundary conditions were external natural convection.

3. Results and discussion

3.1. Temperature imaging of single cell and modules

Results of single cell showed in Fig. 2a and b. Upon charge, the temperature of wires increased firstly and rapidly. Then the temperature of tab and cell inside increased accordingly. The joule heat of wires was sensitive to the current and increased with charge rate from 5C to 10C, 20C, 40C and 60C. Similar, the temperature of tab also increased with charge rate. Since the EDLC type SCs had the symmetric structure for cathode and anode, the temperature of left and right tab always remained the same. Such temperature distribution could be clearly recorded by infrared thermal imager (Fig. 2b).

The inner resistance of cell inside was quite small and the SC cell worked mainly via the adsorption–desorption mechanism, no significant redox reaction existed [2–5,22]. As shown in Figure SI-1, reversible temperature shift owing to the charge and discharge cycle can be clearly recorded under low charge density (0.9 °C at 5C, 0.6 °C at 10C and 20C), where the recording sensitivity or the accuracy of signals of Infrared image was quite quick. It was unable to record under far high charge density (40C and 60C) because the speed of heat transfer and infrared image were difficult to match the charge or discharge rate. Result showed that irreversible temperature shift (caused by joule heat) would exceed reversible temperature shift (caused by adsorption heat) above 10C.

Results of module showed in Fig. 2c and d. Temperature increase was insignificant at 5C. It began to increase at 10C and became much significant at higher C-rates. The environmental temperature increase was changed from less than 0.6 °C as charged at low C-rate (5C-10C) in a short time (4–20 cycles) to 1.0 °C (charged at 20C for 80 cycles) and then to 4.4 °C (charged at 60C for 240 cycles), respectively.

Meanwhile, since the joule heat could be accumulated if without cooling, the temperature for each point sustainably increased with time (Fig. 2c). Temperature in the central of module (B) or near the center (C4) would be higher than that of cells (C1 and C2) far away from the core. The temperature sequences for 5 points of Fig. 1c or Fig. 2 was as follows: B (32.0 °C) > C4 (29.2 °C) > C3 (28.6 °C) > C2 (22.6 °C) > C1 (19.6 °C). Such temperature gradient was due to the heat conduction effect. Thermal accumulation occurred on the circuit board, resulting in a high circuit board temperature which indicated that heat could transferred from the circuit board to each cell.

Similar phenomena were observed as setting the environmental temperature at 7 ~ 8 °C (Figure SI-4). Difference lied in that the temperature of B point was lower and the temperature of C1, C2, C3 and C4 were also much lower. As shown in Fig. 2e1, the environmental temperature exhibited relatively insignificant influences on the heat exchange of the circuit board. On the other hand, the high charge rate (above 60C) had more significant effect of temperature of the cell and the circuit board, comparing the effect of the environmental temperature.

As shown in Figure SI-2 and SI-3, the maximum measurable value of temperature elevation of the cell in module was only 0.6–0.7 °C at 10C and 0.5 °C at 20C. No significant reversible temperature elevation was observed at higher C-rates. The reversible temperature shift of cell in module was similar to that of single cell. Futher more, the result of reversible temperature shift under three conditions showed in Table SI-1. It had no significant relationship with the cell's working state (single or in module) and environmental temperature.

Difference of the temperature elevation between single cell and cell in SCs module (Fig. 2e2) was also observed. Cell in the corner of the module (C1) had the lowest temperature as compared to C2, C3 and C4. But its temperature was still far higher than the single cell without fixed on the circuit board. This temperature difference began to appear at 20C (1.8 °C) and reached its maximum value at 60C (10.3 °C). Combined with the above results, it suggested that Joule heat from the circuit board or wires could influence the temperature rise and temperature differences of cells in module significantly. It was essential to further consider the module's structure or the thermal management methods to control the operating temperature of SCs.

3.2. Origin of the joule heat and the heat sequence of all components on the circuit board

To compare the joule heat effect of wires (on the circuit board) and cell according to Eq.(3), assuming that 1 represented wires and 2 represented cell, then the equation could be written as $\Delta T_1/t_1 = I_1^2 R_1/m_1 Cp_1$, $\Delta T_2/t_2 = I_2^2 R_2/m_2 Cp_2$. Then $I_1 = I_2$, $t_1 = t_2$ because of wires were in series with the cell. Cp_1 was the same order of Cp_2 so that $\Delta T_1/\Delta T_2$ depends on R_1/R_2 and m_1/m_2. For example, we considered wires in Fig. 1b and cell used in the upper experiment. Some parameters were shown on Table SI-2 and Figure SI-5. By calculation, it could be obtained that the minimum resistance of the wires was 1.1 mΩ which with the same order of the resistance of the cell (< 3 mΩ). However, the maximum mass of the wires was 0.42 g, two orders lower than the mass of the cell (75.0 g). Therefore,$\Delta T_1 \gg \Delta T_2$ at the beginning of charge was obtained. It indicated that the smaller mass of the component, the faster heating could be achieved. It also determined the much large thermal flow as studied below.

Considering the temperature increase of the circuit board was the most significant, we further put the focus on the board side (back side) in order to get the much clear information (Figure SI-6a). The back side clearly showed the position of the integrated positive poles and negative poles, the tab of the cell, the wires connecting all cells and resistors for balancing the operating voltage. Note that, when charged at 60C, the temperature of wires increased instantly at 2 s then kept increasing rapidly within several seconds and was 17 °C higher than the environmental temperature at 270 s (infrared images showed in Figure SI-6b). This indicated that joule heat produced on wires was attributed to the instant temperature increase of the wires.

We also measured all temperatures in front side or back side of the circuit board, using two Infrared cameras. As shown in Fig. 3a, for the temperature increase of each component, the sequence was cell (front side) ≈ circuit board (front side) > hot pot on circuit board (wires, tab and resistor) > circuit board (back side) > pole (Fig. 3a2). However, for the speed of temperature increase and decrease, the result showed wires > poles > other parts of circuit board (tab, resistor, back side and front side) > cell (front side), which reflected the order of joule heat intensity (Fig. 3a2 and 3a3). It suggested that the external joule heat on wires and poles can be easily tuned by external measures (such as with cooling or without cooling). In contrast, the temperature change of cell was not easily tuned once it is heated to be a high temperature, considering their large volume and complicated structure. It, in turn, validated the necessity of temperature control of cell to be a reasonable range.

From the result of thermal behavior of the module, a thermal flow pattern on the circuit board was described as Fig. 3b. Joule heat was initialized by wires on the circuit board and then was transferred to the entire circuit board. Thus all cells on the circuit board were simultaneously heated. This heat flow was so huge that resulted in a temperature increase up to 35 °C. The circuit board served as an important

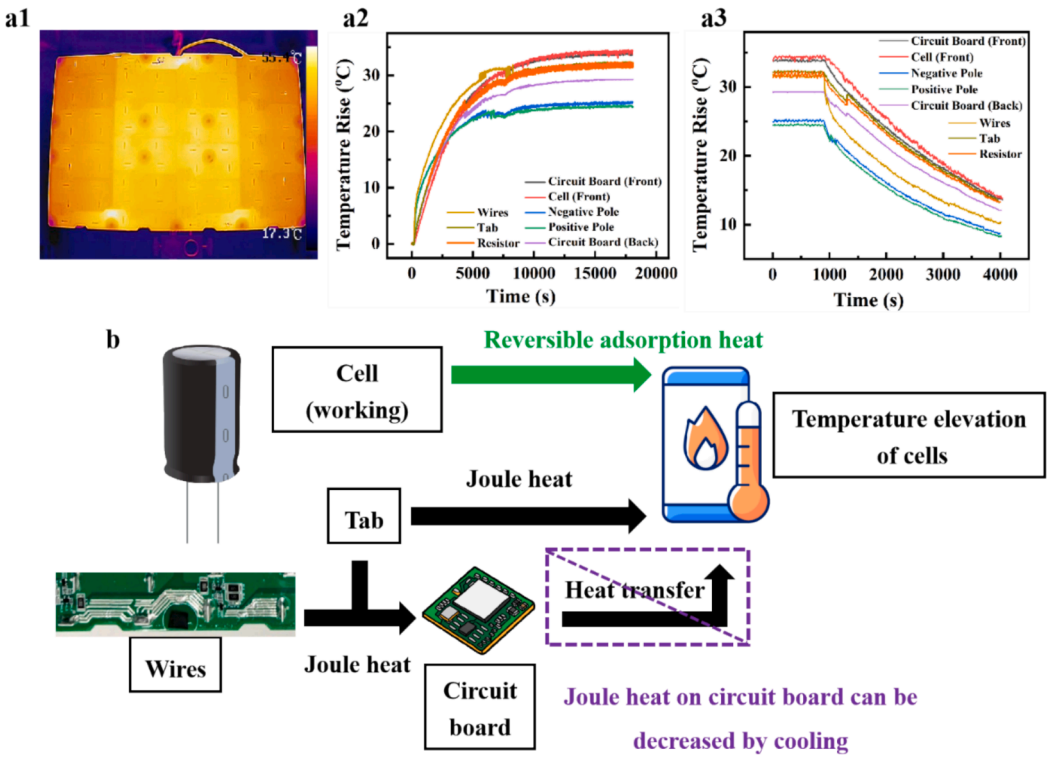


Fig. 3. Thermal behavior of all components on the module; (a1) Infrared image results of back side of the module under the steady state at 60C; (a2) Temperature increase trends with the time for different components or parts; (a3) Temperature decrease trends with the time for different components or parts; (b) Thermal flow pattern on the circuit board.

medium for heat dispersion, conduction and accumulation. In high-power system, it was necessary to consider whether bus bars or other structures could be used as substitutes.

3.3. Effect of temperature increase on SCs performance at different C-rates

Note that, the performance of the cell decayed rapidly with the temperature increase. In general, for single cell with organic electrolyte working at 2.7 V, the life time was up to 10–15 years [2,3,23,24]. The life time would be associated to be 1500 h if constantly working at 65 °C in the accelerating aging test [23]. Considering the performance decay of SCs module was very slow at low charge density, we focused on the temperature elevation effect on the capacitance performance of SCs module after charging at high current density at 60–100C. For charge rate at 60C, temperature with (in the description below, by using fans as shown in Fig. 4b1 and 1d) and without cooling were both recorded. For higher charge rate at 80C and 100C, we only recorded the temperature with cooling. Temperature elevation test without cooling was not carried out from the safety consideration.

Temperature result was shown in Figure SI-7. It was clear that the temperature was close to 46 °C by internal joule heat at 80C, which was similar to that of without cooling at 60C. Similar, temperature was higher than 60 °C when charged at 100C with cooling. Percentage of remaining capacitance after 6000 s was 97.8 %, 93.8 %, 90.1 % at 60C, 80C and 100C respectively (Fig. 4c). Apparently, the decay under higher C-rates would become much serious, which may unbearable if considering the standard exhibited at accelerated aging test (decay should be smaller than 20 % after 65 °C for continuous 1500 h).

Second, in addition to the influence of C-rates, we found that Joule effect also had an impact on the capacitance fade. To consider the impact of Joule heat, a control experiment to eliminate Joule heat needed to be set up. As shown in Fig. 3b, if appropriate cooling strategies were used, the heat flow can be weakened or blocked. Considering the cell once heated was very difficult to cool, it stressed the urgent importance to detect the temperatures of both the cell side and circuit side for any abrupt factor arising joule heat. Firstly, we ventilated the both sides of the circuit board equally to compare the cooling rate between the circuit board and the capacitor (Fig. 4a1). The position in this experiment was C1 at (1,4), C2 at (2,5), C3 at (3,4), C4 at (4,5) and B between (2,4), (2,5), (3,4) and (3,5). Actually, after the charge at 60C for (12000 s), the temperature at B point was 40 °C (Fig. 4a3). As wind was blown from the top, as well as maintaining the charge for 160 cycles, temperatures of each point decreased drastically (Fig. 4a3). Temperature decreases of B, C4, C3, C2, C1, E were 17.5, 7.5, 9.5, 12.5, 14, 3.5 °C within 2000 s, respectively. Intuitive temperature distribution can be clearly recorded by infrared thermal imager (Fig. 4a2). Apparently, circuit board, which didn't generate heat itself, was most easy to be cooled. While, cell (C4) at the core was the most difficult to be cooled. Apparently, cooling measure was necessary in charge and discharge, which was effective to control the temperature to be a safe level. It will also be useful for maintaining the life time of SCs modules (high state of health (SOH) value).

Circuit boards were easy to be cooled, indicating that the influence of Joule heating could be eliminated through gentle cooling. Therefore, two fans (Fig. 4b1 and 1d) with gross power of 40 W was used to make the experiments to ensure the impact of Joule heating can be fully eliminated. The energy consumption for cooling would be 0.8 % that of the cell stored energy at 60C (36F, 4.8 kg, energy density: 2.6 Wh/kg, power density: 0.5 kW/kg). The cooling energy consumption ratio of SCs modules would be the same order as that of Li-ion battery package for vehicles.

Joule heating effect exhibited the rapid temperature increase in the initial working stage of the cell (Fig. 4b3). Temperature increased from 20 °C at 0 s to 47.5 °C at 6000 s. Meanwhile, the associated capacitance of SCs module decreased from 18.22F to 18.09F. In comparison, if the SCs module was cooled by fan wind on the back side, as shown in Fig. 4b2, the high temperature zone caused by Joule heat was limited to

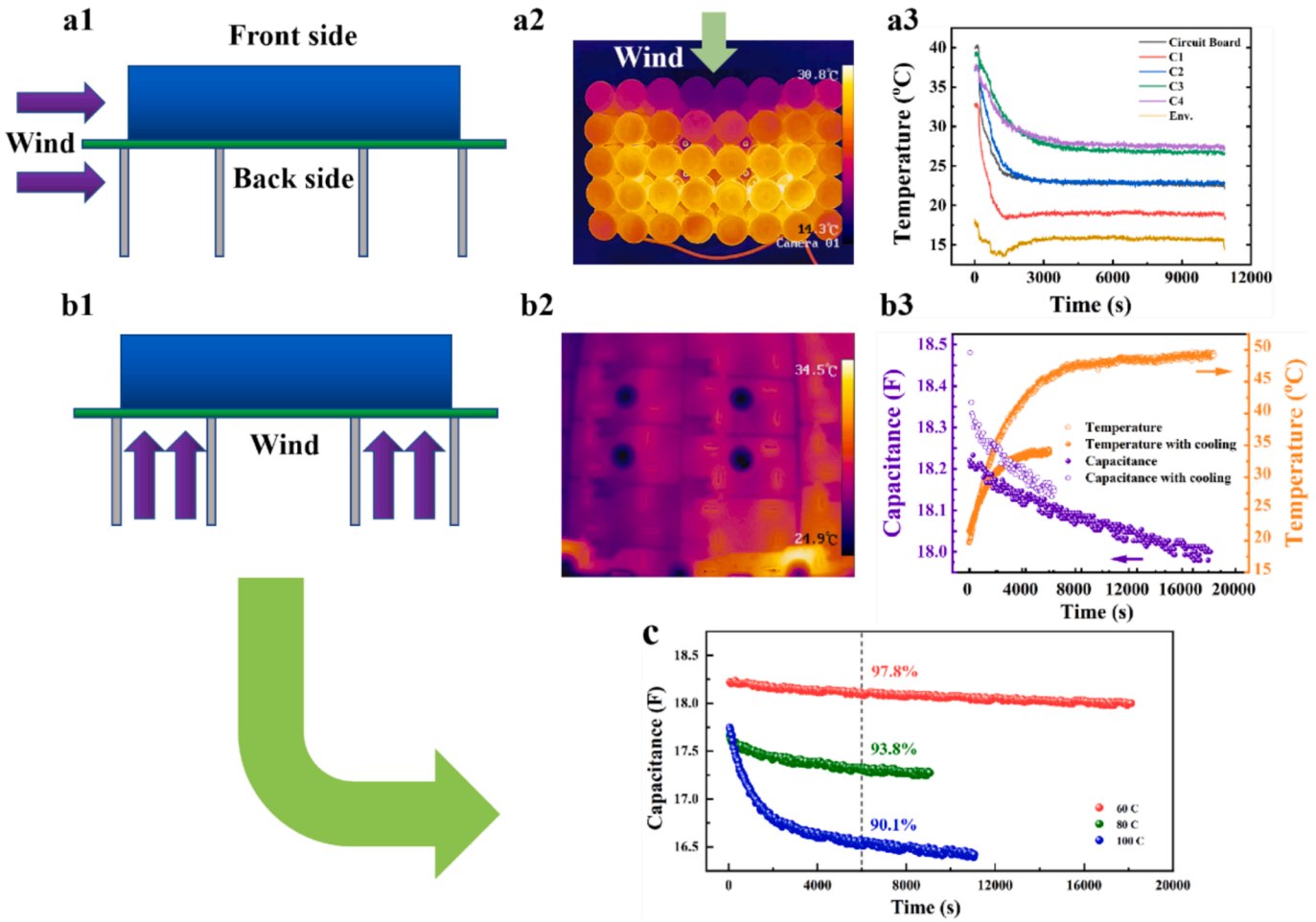


Fig. 4. Temperature and capacitance under different cooling method and C-rates; (a) Schematic of cooling on the two sides (20 W) and temperature result; (b) Schematic of cooling on the circuit side (40 W) and temperature result, capacitance result with and without cooling; (c) comparison of capacitance at 60C and 80C, 100C with cooling.

a small range at the hot spot of the circuit board, which had no effect on cells, the temperature was increased from 20 °C at 0 s to 35 °C at 6000 s. Meanwhile, the associated capacitance decreased from 18.48F to 18.15F. Apparently, Joule heat made the SC module had a lower starting capacitance value. The capacitance without cooling was always lower than that with cooling, which indicated that if a proper cooling system was not established, the impact of Joule heat could be significant.

3.4. Simulation studies on irreversible heat of module

To quantitatively compare the heat generation of circuit boards and cells, a module heat generation model was established. In order to verify the accuracy of the simulation results, the simulation results of the cell and module were compared with the experimental values. As shown in Fig. 5c, for the temperature rise of the tabs, the experimental and simulation results were highly consistent within 5 ~ 60C so that the heating at this point fully conformed to Joule heating characteristics. For temperature of the cylinder, although the numerical values of the simulation results were relatively accurate, it was slightly higher than the experimental results, indicating that the heat generation calculated according to the Joule heating equation ($Q \propto i^2$) was relatively high and there were parts where $Q \propto i^x, x < 2$. Simulation results showed that the temperature rise of single cell conform to the Joule heating law and the simulation and experimental results had a high degree of agreement at different C-rates (Fig. 5c), and the highest temperature was located near the tab (Fig. 5a) because it gathered all the current, similar to Fig. 2b5. In addition, the area outside the tab showed a temperature distribution. Higher temperature near the pole indicated the influence of Joule heat conduction. Module was further scaled with 40 cells and an additional circuit board (Fig. 5b). In addition to cells, a heat source to the circuit board was applied. Temperature distribution was shown in Fig. 5b, similar to Fig. 2d5. Temperature of the tab was slightly lower than the overall temperature of the circuit board, indicating that the cell was heated up by the circuit board and tab was one of the heat transfer media. When changing at different C-rates, the experimental and simulation results could still match with the maximum temperature difference < 2.5 °C (Fig. 5d), suggested that the thermal behavior of the module followed the Joule heating law. If the circuit board heat source power that caused the temperature rise and temperature distribution results was taken as the actual heating power of the circuit board and compared with the total heating power of 40 cells, as shown in Fig. 5e, the heat generation of circuit board was 2–3 times than that of the single cell. Such huge heat flow caused a hidden danger to the working performance and security of the module.

3.5. Insight on the thermal management of SCs modules or SCs system

The present study suggested that temperature management was crucial to the SCs modules, even if single cell of SCs produced very little internal Joule heat. Necessary connection of various cells and the device management add much complicated factors arising external Joule heat. In addition, temperature inside the cell was very difficult to decrease even switching the charge state to be discharge state, because of the frequent charge and discharge operation. In sharp contrast, temperature

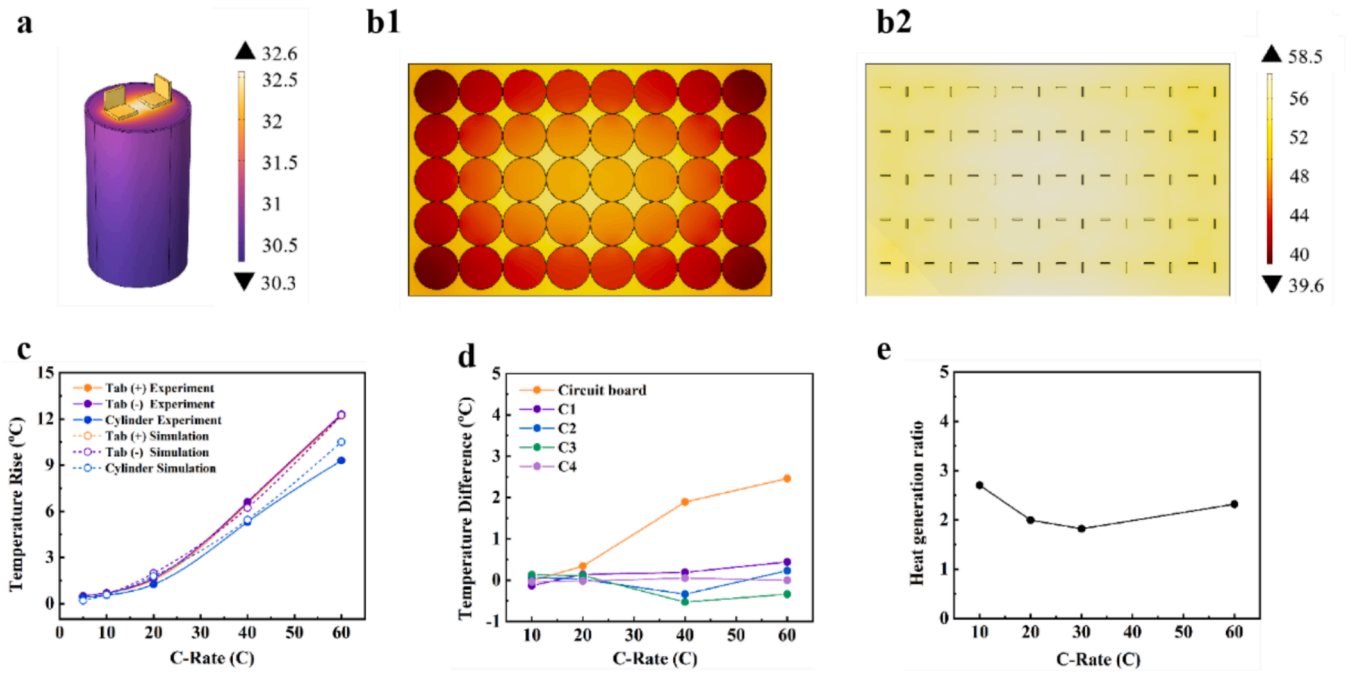


Fig. 5. Simulation results of single cell and module; (a) Temperature distribution of single cell at 60C; (b) Temperature distribution of front and back side of the module; (c) Comparation of the simulation and experimental result of the temperature of single cell; (d) Comparation of the simulation and experimental result of the temperature of module; (e) Heat generation ratio of the circuit board and cells.

of circuit board can be cooled down by wind blowing.

First, these facts suggested clearly that the heat transfer of the SC module should be seriously considered. For long times, the temperature increase of SC was thought to be insignificant, but it was not the case for continuous charge at high current density. Experiments suggested natural cooling may be insufficient and strong convective heat transfer by wind blowing or water cooling in the presence of heat transfer channels was needed, as validated by here and in the battery system [19,25,26]. As revealed in the present work, temperature increase up to 30–40 °C occurred instantly on a circuit board, thus the power for cooling would be very huge with remarkable energy consumption for a SC system up to 1 MW or much larger. These deserve the further investigation.

Second, it was necessary to reduce the use of wires as much as possible, since the connected wires were easily heated by joule heat. Thus, the measurement or detection of each cell in a huge system via the wire network may not be a good solution with a purpose of obtaining the state of charge (SOC) or the SOH of each cell [27,28]. The wires in large amount for measurement not only increase the mass load, decrease the mass energy density and increase the package cost, but also arise uncontrollable thermal risk.

Third, thermal couple was always used in the external shell of the module or wrapped with the cell [29,30], which sensitivity or measurement error was 2–3 °C. Thermal couple was unable to detect the cells which were not connected. In comparison, Infrared camera was able to detect all cells on the circuit board and to give a detecting sensitivity of 0.2–0.3 °C. It was typically important for large scale energy storage system with numerous cells. For the viewpoint of detection sensitivity, IR camera was suitable for the monitoring for determining the reasonable charge density for SCs modules, even in the presence of external cooling measures.

4. Conclusion

An *in situ* Infrared temperature imaging method and simulation model was developed for SC module fixed on a circuit board. Temperature monitoring as charged from 5C to 60C for 240 cycles suggested that Joule heat was firstly initialized on the connecting wires and transferred to the entire circuit board and finally reached each cell. The Joule heat generated by the circuit board was 2–3 times than that of the capacitors. Core position of the circuit board would have the highest temperature if without the cooling measures. Such heat flow was huge to make the cell temperature increase up to 35 °C, far higher than the temperature increase (0.5–0.7 °C) by the reversible adsorption–desorption heat inside the cell. Temperature elevation also resulted in the fast decay of capacitance of SC modules with an unbearable decreasing rate as charged at 60–100 C. The results indicated that Joule heating effect of electronic components such as wires during design was needed to be considered. However, Joule heat could be quickly quenched by the wind blowing, while temperature inside the cell was insensitive to the external cooling measures. Such finding provided anew insight on the temperature monitoring of SC module, stressed the flexible operation mode for huge SC system for safety issue and stressed the design of a reasonable system with bearable cooling energy consumption.

5. Supporting information

Supporting information for this article is given via a link at the end of the document.

Declaration of competing interest

The authors declare that they have no known competing financial interests or personal relationships that could have appeared to influence the work reported in this paper.

Acknowledgements

The project was supported by the National Natural Science Foundation of China (No. 22109085), Huadian group project (CHDER/ELEX-CG-2023-0003). The authors are grateful to Dr. Gang Zhang, Engineer Luming Qian from ZTT corporation for the kind provision of SCs modules for the test.

Appendix A. Supplementary material

Supplementary data to this article can be found online at https://doi.org/10.1016/j.applthermaleng.2024.124684.

Data availability

Data will be made available on request.

References

[1] Q. Li, Y. Zhang, X. Guo, G. Zhang, Y. Yang, M. Du, T. Lv, H. Zhou, Y. Fan, Y. Chen, Y. Wang, H. Pang, Layered (AlO)2OH·VO3 composite superstructures for ultralong lifespan aqueous zinc-ion batteries, J. Colloid Interface Sci. 663 (2024) 697–706, https://doi.org/10.1016/j.jcis.2024.02.189.

[2] Z. Yang, J. Tian, Z. Yin, C. Cui, W. Qian, F. Wei, Carbon nanotube- and graphene-based nanomaterials and applications in high-voltage supercapacitor: A review, Carbon 141 (2019) 467–480, https://doi.org/10.1016/j.carbon.2018.10.010.

[3] M. Inagaki, H. Konno, O. Tanaike, Carbon materials for electrochemical capacitors, J. Power Sources 195 (2010) 7880–7903, https://doi.org/10.1016/j.jpowsour.2010.06.036.

[4] R. Kötz, M. Carlen, Principles and applications of electrochemical capacitors, Electrochim. Acta 45 (2000) 2483–2498, https://doi.org/10.1016/S0013-4686(00)00354-6.

[5] S. Zhang, B. Li, C. Cui, W. Qian, Y. Jin, The progress and comprehensive analysis of supercapacitors for alternating current line filtering: a review, Batteries Supercaps 6 (2023) e202200566, https://doi.org/10.1002/batt.202200566.

[6] Z. Yang, J. Tian, Z. Ye, Y. Jin, C. Cui, Q. Xie, J. Wang, G. Zhang, Z. Dong, Y. Miao, X. Yu, W. Qian, F. Wei, High energy and high power density supercapacitor with 3D Al foam-based thick graphene electrode: Fabrication and simulation, Energy Storage Mater. 33 (2020) 18–25, https://doi.org/10.1016/j.ensm.2020.07.020.

[7] S. Zhang, Z. Yang, C. Cui, X. Chen, Y. Yu, W. Qian, Y. Jin, Ultrafast nonvolatile ionic liquids-based supercapacitors with al foam-enhanced carbon electrode, ACS Appl. Mater. Interfaces 13 (2021) 53904–53914, https://doi.org/10.1021/acsami.1c15754.

[8] Y. Sun, H. Ji, Y. Sun, G. Zhang, H. Zhou, S. Cao, S. Liu, L. Zhang, W. Li, X. Zhu, H. Pang, Synergistic effect of oxygen vacancy and high porosity of nano MIL-125 (Ti) for enhanced photocatalytic nitrogen fixation, Angew. Chem. Int. Ed. 63 (2024) e202316973.

[9] Q. Meng, Y. Huang, L. Li, F. Wu, R. Chen, Smart batteries for powering the future, Joule 8 (2024) 344–373, https://doi.org/10.1016/j.joule.2024.01.011.

[10] W. Zhou, Z. Liu, W. Chen, X. Sun, M. Luo, X. Zhang, C. Li, Y. An, S. Song, K. Wang, X. Zhang, A review on thermal behaviors and thermal management systems for supercapacitors, Batteries 9 (2023).

[11] A. Bothe, A. Balducci, Thermal analysis of electrical double layer capacitors: Present status and remaining challenges, J. Power Sources 548 (2022) 232090, https://doi.org/10.1016/j.jpowsour.2022.232090.

[12] P.H. Smith, T.N. Tran, T.L. Jiang, J. Chung, Lithium-ion capacitors: Electrochemical performance and thermal behavior, J. Power Sources 243 (2013) 982–992, https://doi.org/10.1016/j.jpowsour.2013.06.012.

[13] J. Schiffer, D. Linzen, D.U. Sauer, Heat generation in double layer capacitors, J. Power Sources 160 (2006) 765–772, https://doi.org/10.1016/j.jpowsour.2005.12.070.

[14] Y. Zhang, Z. Liu, X. Sun, Y. An, X. Zhang, K. Wang, C. Dong, Q. Huo, T. Wei, Y. Ma, Experimental study of thermal charge–discharge behaviors of pouch lithium-ion capacitors, J. Energy Storage 25 (2019) 100902, https://doi.org/10.1016/j.est.2019.100902.

[15] O. Munteshari, J. Lau, A. Krishnan, B. Dunn, L. Pilon, Isothermal calorimeter for measurements of time-dependent heat generation rate in individual supercapacitor electrodes, J. Power Sources 374 (2018) 257–268, https://doi.org/10.1016/j.jpowsour.2017.11.012.

[16] H. Li, H. Yang, J. Yan, K. Cen, K. Ostrikov, Z. Bo, Energy and entropy generation analysis in a supercapacitor for different operating conditions, Energy 260 (2022) 124932, https://doi.org/10.1016/j.energy.2022.124932.

[17] R.C. Sahin, S. Gocmen, E. Cetkin, Thermal management system for air-cooled battery packs with flow-disturbing structures, J. Power Sources 551 (2022) 232214, https://doi.org/10.1016/j.jpowsour.2022.232214.

[18] S. Rashidi, N. Karimi, B. Sunden, K.C. Kim, A.G. Olabi, O. Mahian, Progress and challenges on the thermal management of electrochemical energy conversion and storage technologies: Fuel cells, electrolysers, and supercapacitors, Prog. Energy Combust. Sci. 88 (2022) 100966, https://doi.org/10.1016/j.pecs.2021.100966.

[19] I. Voicu, H. Louahlia, H. Gualous, R. Gallay, Thermal management and forced air-cooling of supercapacitors stack, Appl. Therm. Eng. 85 (2015) 89–99, https://doi.org/10.1016/j.applthermaleng.2015.04.003.

[20] X. Hu, Y. Tian, K. Yang, G. Ruan, Design and optimization of air-cooled heat dissipation structure of an on-board supercapacitor box, Appl. Therm. Eng. 249 (2024) 123458, https://doi.org/10.1016/j.applthermaleng.2024.123458.

[21] I. Voicu, R. Rizk, H. Louahlia, F. Bode, H. Gualous, Experimental and numerical study of supercapacitors module with air-cooling, Appl. Therm. Eng. 159 (2019) 113903, https://doi.org/10.1016/j.applthermaleng.2019.113903.

[22] C. Cui, W. Qian, Y. Yu, C. Kong, B. Yu, L. Xiang, F. Wei, Highly electroconductive mesoporous graphene nanofibers and their capacitance performance at 4 V, Journal of the American Chemical Society 136 (2014) 2256–2259, https://doi.org/10.1021/ja412219r.

[23] P.W. Ruch, D. Cericola, A. Foelske, R. Kötz, A. Wokaun, A comparison of the aging of electrochemical double layer capacitors with acetonitrile and propylene carbonate-based electrolytes at elevated voltages, Electrochim. Acta 55 (2010) 2352–2357, https://doi.org/10.1016/j.electacta.2009.11.098.

[24] Z. Ye, S. Zhang, X. Chen, J. Wang, Y. Jin, C. Cui, L. Zhang, L. Qian, G. Zhang, W. Qian, Carbon-al interface effect on the performance of ionic liquid-based supercapacitor at 3 V and 65 oC, J. Electrochem. 28 (2022) 2219005, https://doi.org/10.13208/j.electrochem.2219005.

[25] F. Bahiraei, A. Fartaj, G.-A. Nazri, Electrochemical-thermal modeling to evaluate active thermal management of a lithium-ion battery module, Electrochim. Acta 254 (2017) 59–71, https://doi.org/10.1016/j.electacta.2017.09.084.

[26] H.A. Hasan, H. Togun, A.M. Abed, N. Biswas, H.I. Mohammed, Thermal performance assessment for an array of cylindrical Lithium-Ion battery cells using an Air-Cooling system, Appl. Energy 346 (2023) 121354, https://doi.org/10.1016/j.apenergy.2023.121354.

[27] M. Ceraolo, G. Lutzemberger, D. Poli, State-of-charge evaluation of supercapacitors, J. Energy Storage 11 (2017) 211–218, https://doi.org/10.1016/j.est.2017.03.001.

[28] H. Li, J. Peng, Y. Zhou, J. He, Z. Huang, L. He, J. Pan, SoH-aware charging of supercapacitors with energy efficiency maximization, IEEE Trans. Energy Convers. 33 (2018) 1766–1775, https://doi.org/10.1109/TEC.2018.2841427.

[29] H. Gualous, H. Louahlia-Gualous, R. Gallay, A. Miraoui, Supercapacitor thermal modeling and characterization in transient state for industrial applications, IEEE Trans. Ind. Appl. 45 (2009) 1035–1044, https://doi.org/10.1109/TIA.2009.2018879.

[30] M. Al Sakka, H. Gualous, J. Van Mierlo, H. Culcu, Thermal modeling and heat management of supercapacitor modules for vehicle applications, J. Power Sources 194 (2009) 581–587, https://doi.org/10.1016/j.jpowsour.2009.06.038.